Mon. Not. R. Astron. Soc. **000**, 1–15 (2011) Printed 18 July 2011 (MN LATEX style file v2.2)

Testing the *WMAP* cosmology via *Planck* radio catalogues

J.R. Whitbourn[1⋆], T. Shanks[1]† and U. Sawangwit[1]‡
[1] *Department of Physics, Durham University, South Road DH1 3LE*

Accepted ; Received ; in original form

ABSTRACT

The prime evidence underpinning the standard ΛCDM cosmological model is the CMB power spectrum as observed by *WMAP* and other microwave experiments. But Sawangwit & Shanks have recently shown that the *WMAP* CMB power spectrum is highly sensitive to the beam profile of the *WMAP* telescope. Here, we use the source catalogue from the *Planck* Early Data Release to test further the *WMAP* beam profiles. We confirm that stacked beam profiles at Q, V and particularly at W appear wider than expected when compared to the Jupiter beam normalised either directly to the radio source profiles or using *Planck* fluxes. The same result is also found based on NVSS and *WMAP* 'CMB-free' source catalogues. Further, the *WMAP* source fluxes demonstrate a non-linear relation with *Planck* fluxes, as previously found between *WMAP* and ground-based fluxes. Importantly, we find that applying this non-linear relation to the Jupiter beam profile results in an excellent fit to the observed radio source profiles. Also, stacked SZ decrements of ≈ 160 galaxy clusters observed by *Planck* appear to be underestimated in the *WMAP* data by a factor of ≈ 2 in the Q, V and W bands. The strength of this discrepancy at Q means that it cannot be fully explained by the beam profile problem and thus the *WMAP* SZ discrepancy remains unexplained. Beam profile systematics can have significant effects on both the amplitude and position of the first acoustic peak. In particular, a wider beam can move the position of the first peak to significantly larger wavenumbers with potentially important implications for cosmology.

Key words: methods: analytical - galaxies: general - cosmic microwave background - cosmology, large-scale structure of Universe

1 INTRODUCTION

CMB experiments such as *WMAP* have made significant progress in the study of the primordial temperature fluctuations. Their best fitting power spectra strongly support a spatially flat, ΛCDM, universe. This model requires relatively few parameters, yet apparently manages a compelling concordance between a variety of other cosmological data; SNIa, Large Scale Structure and Big Bang Nucleosynthesis. Although the statistical errors on these power spectra are small, this precision does not necessarily imply accuracy and there remains the potential for systematic errors to alter these conclusions.

Indeed, several anomalies between ΛCDM and the *WMAP* data have been discussed. Typically these have involved the large-scale temperature multipoles eg: (Bennett et al. 2011). However, other anomalies in the CMB at smaller scales have also been detected, connected in particular with radio sources (Sawangwit & Shanks 2010a,b) and SZ decrements from galaxy clusters (Myers et al. 2004; Bielby & Shanks 2007)

Radio sources are sometimes regarded as a contaminant in CMB temperature maps. However, radio point sources prove particularly interesting because they provide a complementary check of the beam measured by the *WMAP* team from observations of Jupiter (Page et al. 2003; Hill et al. 2009). Jupiter has a flux of ≈ 1200Jy which is ≈ 3 orders of magnitude higher than radio source fluxes or CMB fluctuations. This high flux has advantages in terms of defining the wings of the beam profile but is a disadvantage in that the calibrating source is much brighter than typical CMB fluctuations. Furthermore, Jupiter only checks the beam on the ecliptic whereas radio sources are spread over the sky. Sawangwit & Shanks (2010a,b) made a stacked analysis of radio point sources and found evidence for a wider beam than *WMAP* measured using Jupiter. A tentative detection of a non-linear relation between *WMAP* fluxes and ground based radio telescope fluxes was also found. A

⋆ E-mail: (JRW) joseph.whitbourn@durham.ac.uk
† E-mail: (TS) tom.shanks@durham.ac.uk
‡ E-mail: (US) utane.sawangwit@durham.ac.uk

thorough analysis of possible systematics did not find an explanation and we return to these issues later in this paper. The beam profile of a CMB telescope like *WMAP* is critical because it smoothes the temperature anisotropies and therefore needs to be known accurately to produce the final power spectrum from temperature maps (Page et al. 2003; Hill et al. 2009).

Various authors have noted small-scale anomalies with respect to the SZ decrements measured by *WMAP*. SZ decrements are created when the CMB inverse Compton scatters off hot electrons in galaxy clusters. Myers et al. (2004) first stacked *WMAP* data at the positions of galaxy clusters and suggested that the profiles were more extended than expected. Lieu, Mittaz, & Zhang (2006) and Bielby & Shanks (2007) then found that the SZ decrements from *WMAP* were reduced compared to X-ray predictions, possibly due to the *WMAP* beam being wider than expected. Bielby & Shanks (2007) also found that the *WMAP* decrements were 3-5σ lower than the ground-based SZ measurements by Bonamente et al. (2006) in 38 X-ray luminous clusters. These anomalous *WMAP* SZ results have been confirmed by a variety of re-analyses, (e.g. Diego & Partridge 2009), including a stacking analysis by the *WMAP* team (Komatsu et al. 2011).

In their ESZ sample, the *Planck* team find excellent agreement with the self-similar X-ray estimates of the SZ decrement (Planck Collaboration et al. 2011). This is corroborated by the ground based South Pole Telescope Collaboration with their blind SZ selected cluster sample (Mroczkowski et al. 2009). This compounds the question of why *WMAP* SZ analyses from Lieu, Mittaz, & Zhang (2006) and Bielby & Shanks (2007) failed to find such an agreement. Although Komatsu et al. (2011) claimed the *WMAP* discrepancy was only a 1.5-2σ effect, they focussed on comparing the integrated Y parameter rather than the inner SZ profile which generally shows a more significant discrepancy (Bielby & Shanks 2007).

In this paper we use the recent Planck Early Data Release and other radio source data to re-investigate both the *WMAP* radio source beam profile and SZ anomalies. The Planck Early Release Compact Source catalogue (ERCSC) is of particular interest and provides the basic parameters of radio sources and SZ clusters from the *Planck* CMB maps. Although, the corresponding temperature maps from which these were estimated have not been released, both radio source fluxes and SZ profile parameters are available as measured by *Planck*. We can therefore use these to compare *WMAP* and *Planck* radio source fluxes directly and also to make *WMAP* stacks centred now on the new radio source and SZ cluster lists from *Planck*. From these stacks, the *WMAP* beam profile can be inferred and the SZ results from *WMAP* and *Planck* compared. Given the higher angular resolution, lower noise and different calibration strategy for *Planck*, this comparison will allow new insight into the robustness of the *WMAP* CMB analysis.

2 DATA

2.1 Planck Early Data Release

The *Planck* team have recently made their first release of data collected by the *Planck* satellite between 13 August 2009 and 6 June 2010 (amounting to $\approx$ 1.5 full sky surveys). This early data release is concerned solely with the foreground contamination in the CMB maps. The two sets of catalogues relevant to this paper form the Early Release Compact Source catalogue (ERCSC). These are the Radio Source catalogues and the SZ catalogue.

2.1.1 Planck Radio Sources

The Early Release Compact Source Catalogue (ERCSC) lists all the high reliability radio sources with accurate flux determinations. The ERCSC has been quality controlled so that $\geqslant 90\%$ of the reported sources are reliable, $> 5\sigma$ detections and that the fluxes are determined within $\leqslant 30\%$ accuracy. The catalogues are band specific and for the bands of interest ($\nu \leqslant 100GHz$) are created using the 'PowellSnakes' method, a Bayesian multi-frequency algorithm for detecting discrete objects in a random background. Flux estimates were obtained by use of aperture photometry within a circle of the beam's FWHM. For the case of unresolved and potentially faint point sources, the *Planck* team recommend the use of the parameter FLUX and its corresponding error, FLUX_ERR (Planck Collaboration et al. 2011).

We reject any extended objects from the catalogue to maintain an unresolved sample with which to test the *WMAP* beam profile. To do this we make use of the *Planck* quality tag 'EXTENDED'. This is defined by comparing the source areal profile with the 2-D *Planck* beam. An additional quality flag 'CMBSUBTRACT' has also been provided, which reflects on the quality of the source detection in a map with the best estimate of the CMB removed. In this paper we reject any sources with a value of 2, as the *Planck* team recommend, (Planck Collaboration et al. 2011).

We have also rejected sources within 4° of the LMC and sources at low galactic latitude, $|b| < 5°$. We also rejected sources flagged with high astrometric error and any sources with *WMAP* counterparts that are flagged as contaminated.

Band corrections between *WMAP* and *Planck* have been ignored in the absence of information on the spectral index. This factor is in any case small (Planck Collaboration et al. 2011). The full details of the catalogue construction and composition are described by *Planck* Collaboration et al. (2011) and briefy overviewed in Table 2.2. The number of sources, N, selected in each bandpass are also shown in this Table.

2.1.2 Planck SZ Catalogue

The Early SZ (ESZ) catalogue lists all the robust and extensively verified SZ detections in the first data release. As described by Melin, Bartlett, & Delabrouille (2006), the *Planck* team extract the integrated Y parameter using a Multifrequency Matched filter (MMF3) method (*Planck* Collaboration et al. 2011). The algorithm is run blindly on all-sky maps, assuming the characteristic SZ spectral signature and self-similar cluster profile.

In the Early Release of the *Planck* SZ catalogue, only data from the 100GHz frequency channel or higher has been used to study the SZ effect. This is to avoid the deterimental effect on S/N from beam dilution caused by the larger beam sizes of the lower frequency channels. At the higher frequencies, the *Planck* beam FWHM is typically $\approx 4.'5$. The full

Freq [GHz]	FWHM ($'$)	N	Flux Limit [Jy]
100	9.94	251	0.344
70	13.01	134	0.481
44	27.00	114	0.781

Table 1. Summary of the *Planck* bandpass parameters and the flux range of the sample we use from the ERCSC after we have taken our quality cuts, (Planck Collaboration et al. 2011). N is the number of radio sources to the specified limit.

Band	Freq [GHz]	FWHM ($'$)	Ω (sr)	Γ^{ff} $[\mu KJy^{-1}]$	$g(\nu)$
W	94	12.6	$2.097{\cdot}10^{-5}$	179.3	1.245
V	61	19.8	$4.202{\cdot}10^{-5}$	208.6	1.099
Q	41	29.4	$8.978{\cdot}10^{-5}$	216.6	1.044

Table 2. Summary of the *WMAP* bandpass parameters taken from Hill et al. (2009) and Jarosik et al. (2011). See text for definitions.

details of the catalogue construction and composition are described in *Planck* Collaboration et al. (2011).

The catalogue provides estimates of the SZ flux, extent, redshift and position. It consists of 189 clusters, all detected at high S/N ($\geqslant 6$) with 95% reliability. Whilst the sample is primarily composed of known clusters (169/189), it provides a wealth of new information as it gives the first SZ measurements for $\approx 80\%$ of the clusters. In this paper we only make use of clusters with known redshifts and these all have X-ray observations. We therefore consider 159 clusters, including Coma. For this sample the redshift range spans $z \in [0.0126, 0.546]$ with a mean redshift of $\overline{z} = 0.179$.

2.2 *WMAP* Data

We will be using the 7-year *WMAP* temperature maps obtained from the LAMBDA CMB resource. We work with the $N_{side} = 512$ Healpix maps resulting in a pixel scale of $7'$. We use the foreground unsubtracted temperature band maps for Q,V and W. We estimate the Jupiter beam in each band by averaging the 7-year beam profiles from the various DA's. To avoid Galactic synchrotron contamination we have used the extended temperature mask which admits 71% of the sky. When working with radio point sources we instead use the point source catalogue mask.

We have used the 7-year *WMAP* point source catalogue. These sources are detected at least the 5σ level in one *WMAP* band. For a flux density to be stated, the detection must be above the 2σ level in that band. Following Sawangwit & Shanks (2010a) we ensure that the sources are genuinely point source by matching to the 5GHz ($\approx 4'.6$ resolution) catalogues from the Greenbank Northern sky Survey (GB6), Gregory et al. (1996), or Parkes-MIT-NRAO (PMN), Griffith & Wright (1993), surveys. The *WMAP* team also provide a 7 yr CMB-free catalogue as described by Gold et al. (2011). This catalogue has been created with the objective of detecting point sources free of boosting by CMB fluctuations. After the 5GHz matching, we proceed with a raw catalogue with 471 sources and a CMB-free catalogue with 417 sources.

3 *PLANCK* RADIO SOURCE FLUXES AND SZ CLUSTER DECREMENTS

3.1 Conversion of Radio Flux to Temperature Profiles

The *Planck* ERCSC provides us with the source flux density, error and a few parameters on the source characterstics and detection. To enable us to translate the *Planck* fluxes into *WMAP* observables we need to convert the source flux density into an observed peak Rayleigh-Jeans temperature using the conversion factor, Γ (Page et al. 2003).

$$\Delta T_{RJ}(0) = S_{tot}\Gamma \tag{1}$$

A simplified form for Γ can be found, Page et al. (2003).

$$\Gamma^{ff} = \frac{c^2}{2k_b\nu_e^2}\frac{1}{\Omega_{beam}} \tag{2}$$

Here ν_e is the effective frequency and Γ^{ff} denotes the fact that the majority of the *WMAP* sources have a power index $\alpha \approx -0.1$, approximately that of free-free emission.

The *WMAP* temperature maps are given in terms of the thermodynamic temperature. At the *WMAP* frequencies and CMB temperature, the Rayleigh-Jeans temperature is appreciably different from this. We therefore correct between the two temperature differences, using eq(3), where $x' = h\nu/k_bT_{cmb}$ and $T_{cmb} = 2.725$K is the monopole temperature of the CMB.

$$\begin{aligned}\Delta T_t &= \frac{(e^{x'}-1)^2}{x'^2e^{x'}}\Delta T_{RJ} \\ &= g(\nu)\Delta T_{RJ}.\end{aligned} \tag{3}$$

The observed *WMAP* temperature profiles therefore take the form,

$$\begin{aligned}\Delta T(\theta) &= \Delta T(0)b^s(\theta) \\ &= g(\nu)\Gamma^{ff}S_{tot}b^s(\theta).\end{aligned} \tag{4}$$

We see the beam dependence of the observed profile is twofold. The shape is dependent on the symmetrized beam profile $b^s(\theta)$ (normalised to unity at $\theta = 0^\circ$), while the scale is normalised by the beam solid angle associated with Γ^{ff}. A summary of the assumed values of $g(\nu)$ and Γ^{ff} are provided in Table 2.

3.2 *Planck* SZ Decrements

Planck presents its observed decrements using an SZ model fit parameterised by the total SZ signal within the cluster extent. Here we briefly describe this model so that the *Planck* results can be compared to the stacked *WMAP* temperature decrements.

Clusters are significant reservoirs of gas which will result in a SZ distortion to the CMB described by the Compton y parameter,

$$\Delta T(\theta) = T_{cmb} j(x') y(\theta) \tag{5}$$

$j(x')$ is the spectral function, where $x' = h\nu/k_b T_{cmb}$ (see e.g. Refregier, Spergel, & Herbig 2000) The integrated Y parameter is the total SZ signal, which is simply the integration of the Compton y parameter on the sky.

$$Y = \int y d\Omega. \tag{6}$$

Alternatively, if we integrate over the cluster volume,

$$Y = \frac{\sigma_t}{m_e c^2} \int P dV. \tag{7}$$

However, we are observing a 2-D projection of the cluster[1] on the sky. The angle θ we observe on the sky, corresponds in 3-D to a cylindrical bore of the cluster of radius $R = \theta D_a(z)$. where D_a is the angular diameter distance. The observed integrated Y parameter therefore takes the form (Arnaud et al. 2010),

$$Y_{cyl}(R) = \frac{\sigma_t}{m_e c^2} \int_0^R 2\pi r dr \int_r^{R_{tot}} \frac{2P(r')r'dr'}{(r'^2 - r^2)^{1/2}} \tag{8}$$

$$= Y_{sph}(R_{tot}) - \frac{\sigma_t}{m_e c^2} \int_R^{R_{tot}} 4\pi P(r)(r^2 - R^2)^{1/2} r dr \tag{9}$$

To predict the SZ effect implied by eq(9) we have to make a choice of the pressure profile $P(r)$. Historically it has been common to fit the SZ profile with an isothermal β model, (Cavaliere & Fusco-Femiano 1976). However, X-ray observations have shown that the assumption of an isothermal gas breaks down at the cluster outskirts, (Pratt et al. 2007; Piffaretti et al. 2005). To account for this additional complexity, Nagai, Vikhlinin, & Kravtsov (2007) therefore proposed using a Generalised NFW (GNFW) profile for the pressure instead. The profile is scale invariant in that it is independent of absolute distances and is instead a function of the dimensionless scale $x = R/R_{500}$. The profile takes the form,

$$\mathcal{P}(x) = \frac{P_0}{(c_{500}x)^\gamma [1 + (c_{500}x)^\alpha]^{(\beta-\gamma)/\alpha}} \tag{10}$$

where $\mathcal{P}(x) = P(r)/P_{500}$ where P_{500} is the characteristic pressure defined by Arnaud et al. (2010).

Here we have a five parameter fit to the pressure profile[2] $[P_0, c_{500}, \gamma, \alpha, \beta]$. This allows independent specification of the pressure in the cluster core (γ), main-body (α) and outskirts (β). In Table 3 we outline the parameters used by *Planck*, as taken from Arnaud et al. (2010). The characteristic parameters of the cluster are M_{500}, P_{500}, R_{500} (see Appendix A) where the 500 denotes the fact they are evaluated within the region where the mean mass density is 500 times greater that the critical density $\rho_{crit}(z)$.

[1] The cluster is assumed to be spherical.

[2] Note the β introduced here is different from the β associated with the isothermal fit to the pressure profile.

Type	P_0	c_{500}	γ	α	β
All:Fitted	$8.403(\frac{h}{0.7})^{-\frac{3}{2}}$	1.177	0.3081	1.0510	5.4905

Table 3. Summary of the *Planck* NFW parameters as used in eqn. 10 and described by Arnaud et al. (2010). These are the same parameters as used by the *Planck* team, the All:Fitted set.

The *Planck* team extract the integrated Y parameter using the Multifrequency Matched Filter (MMF3) method (*Planck* Collaboration et al. 2011) based on the above self-similar model. The integration is done to the angular cluster extent corresponding to $5R_{500}$, which they also report (θ_{5R500}). Their errors on the SZ integrated Y and angular extent, θ_{5R500}, are estimated by iterative re-measurements.

3.3 SZ Temperature Profile Reconstruction

We now proceed to invert the *Planck* data to provide us with expected *WMAP* temperature profiles. (See Appendix A for the details of this derivation). ¿From the *Planck* values for $Y(5R_{500})$[3] and θ_{5R500}, and using $J(x)$ and $I(x)$, the cylindrical and spherical SZ templates (see eqns. A7) we first obtain $Y_{cyl}(R)$ via eqn. A9,

$$Y_{cyl}(R) = Y_{cyl}(5R_{500})\left(1 - \frac{J(x)}{I(5)}\right). \tag{11}$$

From this integrated $Y_{cyl}(R = \theta \cdot D_A(z))$, we want to derive the angular dependence of the Compton y parameter, where $y(\theta) = \frac{d}{d\Omega} Y_{cyl}(\theta)$, and so

$$y(\theta) = -\frac{Y_{cyl}(5R_{500})}{I(5)} \frac{d}{d\Omega}\big(J(x)\big). \tag{12}$$

The self-similar model therefore predicts an SZ temperature decrement,

$$\Delta T_{SZ}(\theta) = T_{cmb} j(x') \frac{Y_{cyl}(5R_{500})}{I(5)} \frac{d}{d\Omega}\big(J(x)\big) \tag{13}$$

where $Y_{cyl}(5R_{500})$ is the integrated Y given in ESZ.

We have corroborated this method with an alternative calculation of $Y_{cyl}(R)$ which is independent of the *Planck* provided $Y(5R_{500})$ and instead solely uses θ_{5R500}. The strategy is to evaluate M_{500}, to find P_{500} using equn. 13 of Arnaud et al. (2010) and hence Y_{500}. $Y_{cyl}(R)$ is the product of this and the cyclindrical scaling function $J(x)$ (see eqn. A5). We find that the inferred SZ profiles between our two methods agree very well with $< 10\%$ difference at all scales with this small difference being caused by the second method's dependence on the $Y - M$ calibration and the specification of the cluster physics.

3.4 Isothermal profiles from SZ parameters

We have seen that the reconstructed *Planck* decrements are actually reasonably insensitive to the SZ template, at least within R_{500}. This even applies when the self-similar model

[3] It is assumed that $Y_{cyl}(5R_{500}) = Y(5R_{500})$

is replaced by an isothermal model. On the basis of Fig. 11 of Arnaud et al. (2010) which compares Y values as estimated from the REXCESS sample, the isothermal model requires a $Y_{5R_{500}}$ parameter $\approx 3\times$ larger than the self-similar model but the $Y_{R_{500}}$ values are more similar. This gives us a route to produce an SZ decrement from the isothermal model based on the measured *Planck* Y value. The isothermal model then has a Compton-y parameter of the form,

$$y(\theta) = y_0 \left[1 + \left(\frac{\theta}{\theta_c}\right)^2\right]^{-\frac{3\beta}{2}+\frac{1}{2}} \quad (14)$$

Equating $Y_\beta(5R_{500}) = 3.2 \times Y_{5R_{500}}$, we solve for the amplitude y_0 using $Y_\beta(5R_{500}) = \int_0^{\Omega(5R_{500})} y(\theta) d\Omega$. We find that

$$y_0 = Y_\beta \left(\frac{-\frac{3\beta}{2}+\frac{1}{2}}{\pi\theta_c^2}\right)\left(\left[1+\left(\frac{\theta_{5R_{500}}}{\theta_c}\right)^2\right]^{-\frac{3\beta}{2}+\frac{3}{2}} - 1\right)^{-1} \quad (15)$$

We can therefore predict the SZ temperature decrement using eq(5) and eq(14). Following Lieu, Mittaz, & Zhang (2006) and Bielby & Shanks (2007) we assume $\theta_c = 9.8'$ and $\beta = 0.75$ from the Coma cluster as typical isothermal model parameters, scaling θ_c with redshift using a $\Omega_\Lambda = 0.7$, $\Omega_m = 0.3$ angular distance relation.

Clearly, the isothermal model may represent the *Planck* results less accurately than the self-similar model from eqn 13. But we shall see that, for fixed integral Y, the isothermal model produces lower central temperatures and it will be interesting to see if that helps the agreement with the *WMAP* stacked SZ decrements.

4 CROSS-CORRELATION METHODS

Our cross-correlation/stacking procedures for measuring both radio point source profiles and SZ decrements are similar to those of Myers et al. (2004), Bielby & Shanks (2007) and then as updated by Sawangwit & Shanks (2010a). Ultimately, we shall be stacking/cross-correlating *WMAP* data around radio source positions and cluster centres from catalogues, particularly from *Planck* ERCSC. To estimate a decrement for an individual source we use,

$$\Delta T(\theta) = \sum_i \frac{T_i(\theta) - \overline{T}}{n_i(\theta)} \quad (16)$$

where the sum is over the pixels, denoted i, within a circular annulus centered on the angular separation θ. n_i represents the number of pixels within the annulus and T_i is the temperature recorded for the pixel i. $\overline{T}$ is the average background temperature which can either be estimated locally in a surrounding annulus in a 'photometric method' or globally (see Sawangwit & Shanks 2010a). These two background estimates make no difference in the stacked results but can make a difference for individual clusters (see Section 8). We then stack the *WMAP*7 data by averaging $\Delta T_j(\theta)$ over sources, j.

We have followed Sawangwit & Shanks (2010a) in using jack-knife errors, for both the radio and SZ sources, based on 6 equal area sub-fields defined by lines of constant galactic longitude and split by the galactic equator. We have also experimented with both alternative sub-fields and methods such as bootstrap resampling, finding approximately equivalent results.

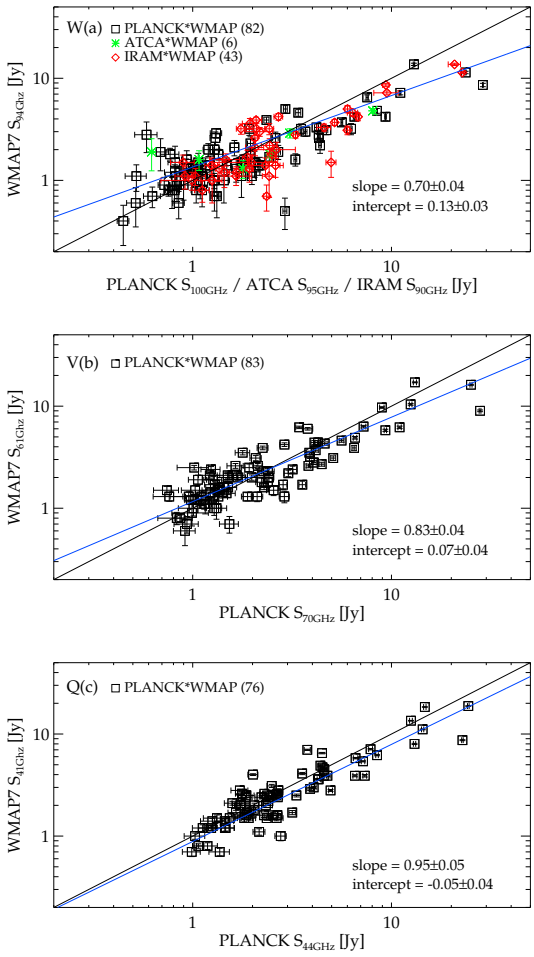

Figure 1. A comparison between the *WMAP*7 fluxes, *Planck* and ground based source fluxes.

5 *PLANCK* RADIO SOURCE RESULTS

5.1 Flux Comparisons

We now compare *WMAP*7 sources at Q, V, W to their counterparts in the *Planck* ERS at 100, 70 and 44 GHz. We also compare the *Planck* fluxes in the 100GHz band to the ground-based ATCA and IRAM source fluxes previously used by Sawangwit & Shanks (2010a).

In Fig. 1 we compare the *WMAP*7 fluxes to *Planck* and the ground-based ATCA and IRAM sources. We only consider the matches with separation less than $2'$ to avoid any possible systematic errors associated with sources that have poor astrometry. However, our results are independent of this cut up to $10'$. At high fluxes we see evidence for a systematically lower *WMAP* flux, $\approx 50\%$ above 2Jy. This non-linearity is particularly prominent in the W band, the band with the greatest angular resolution. This *Planck*-*WMAP* non-linearity is statistically significant in W and V and ro-

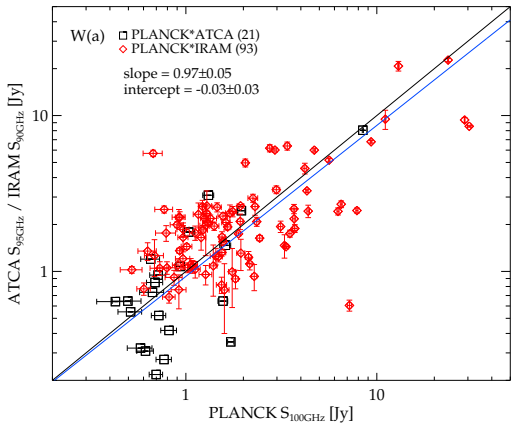

Figure 2. A comparison of the 100GHz *Planck* fluxes and the ground-based sources.

bust to high flux outliers. We find best fit logarithmic slopes of $[0.70 \pm 0.04, 0.83 \pm 0.04, 0.95 \pm 0.05]$ for [W,V,Q]. Thus the one-to-one relation is strongly rejected in both W and V, although not in Q.

Clearly, *Planck* and *WMAP* fluxes for sources were measured at different times. Since at least $\approx 30\%$ of the *WMAP5* radio sources exhibit some level of variability (Wright et al. 2009), we expect and observe much larger scatter than accounted for by the estimated flux uncertainty. We note that since the brighter *WMAP* sources are too faint, this is in the opposite sense expected if variability was biasing faint *Planck* sources into the *WMAP* catalogue when in a bright phase.

The non-linearity between *Planck* and *WMAP* is in contrast to direct comparisons between *Planck* and ground-based data. These instead show good agreement, as shown in Fig. 2 for the *Planck* 100GHz radio point sources. The best fit logarithmic slope of $[0.97 \pm 0.05]$ is statistically consistent with the one-to-one relation. This is particularly significant because this is the frequency band with the greatest *Planck*-*WMAP* non-linearity.

Given this agreement between *Planck* and the ground-based observations, we interpret the flux non-linearity as being due to *WMAP*. In Section 7 we shall relate this problem to the wider than expected beam profiles observed by Sawangwit & Shanks (2010a).

5.2 *Planck* Profiles

We now repeat the stacking analysis of Sawangwit & Shanks (2010a) centring on the *Planck* radio point sources. *Planck* sources are selected at multiple wavebands which may be advantageous in avoiding spurious sources etc. Figs. 3 (a),(b),(c) are shown for completeness because these raw temperature plots demonstrate the main uncertainty in this analysis which is the accuracy of the background subtraction. We note that there is some difference between the global background (dotted line) and the background local to the source samples but generally this effect appears smaller in the *WMAP7* data (eg at W) than it was in the *WMAP5* datasets used by Sawangwit & Shanks (2010a).

Figs. 3 (d),(e),(f) show the same profiles now background subtracted and scaled to unity at the origin to produce $b^S(\theta)$. We have used the 'photometric' subtraction to produce the radio point source temperature profile, $\Delta T_{radio}(\theta)$. For the *WMAP7* dataset there is very little difference in the profiles resulting from global or local/photometric background subtractions.

These $b^S(\theta)$ are now compared to the *WMAP* Jupiter beam and the best fit beam to the bright *WMAP* radio source profiles found by Sawangwit & Shanks (2010a) (dashed orange line in their Fig. 2). There is again evidence that the *Planck* selected radio sources suggest a wider beam than the Jupiter beam, particularly in the W band, although the *Planck* sources lie slightly below the profile fits from Sawangwit & Shanks (2010a). However, statistically, both results are in good agreement.

The normalisation of $b^S(\theta)$ to unity at small scales forms a further uncertainty in these beam comparisons. In Figs. 3 (g),(h),(i) we have applied the formalism of Section 3.1 and attempted to make absolute normalisations of the various model profiles, using the *Planck* ERCSC listed fluxes. Here if the radio sources followed the Jupiter profile, for example, we should see the same peak temperature for the stacked model profile and the stacked data. We see that the *Planck* peak temperatures, particularly in the W band, tend to lie between the Jupiter profile and the previous *WMAP* bright radio source fits. These results suggest that the previous radio source fit may be too wide at $\theta > 30'$ where it is essentially an extrapolation, unconstrained by the data, and this will affect the accuracy of its absolute normalisation i.e. there is a large error in $\Omega_{\rm beam}$. Otherwise, the conclusion is similar to that from Figs. 3 (d),(e),(f) in that the *Planck* data is suggesting that the Jupiter beam is a poor fit to the radio source profiles particularly at W.

6 *WMAP* AND NVSS RADIO SOURCES

6.1 *WMAP7* radio sources

We next repeat the analysis of Sawangwit & Shanks (2010a) for the *WMAP7* data where the S/N is slightly higher than in the *WMAP5* dataset originally used by these authors. We continue to use the *WMAP7* source list of Gold et al. (2011). The results are shown in Fig. 4. We see that the results reasonably agree with the power-laws fitted by Sawangwit & Shanks (2010a). At large scales, the profiles may return to zero more uniformly than previously, making the differences between the photometric and global profile estimates more marginal than previously found.

6.2 *WMAP7* 'CMB-free' radio sources

We take the opportunity to make measurements of the beam profile based on other radio source samples. One suggestion has been that the wider than expected radio source profiles might be caused by Eddington bias. Sawangwit & Shanks (2010a) have already argued against this on the grounds that effectively we selected on the GB6 and PMN ground-based data, and this meant that the profiles might not be widened due to mis-identifying upward CMB fluctuations in the *WMAP* maps as CMB sources. We now check this

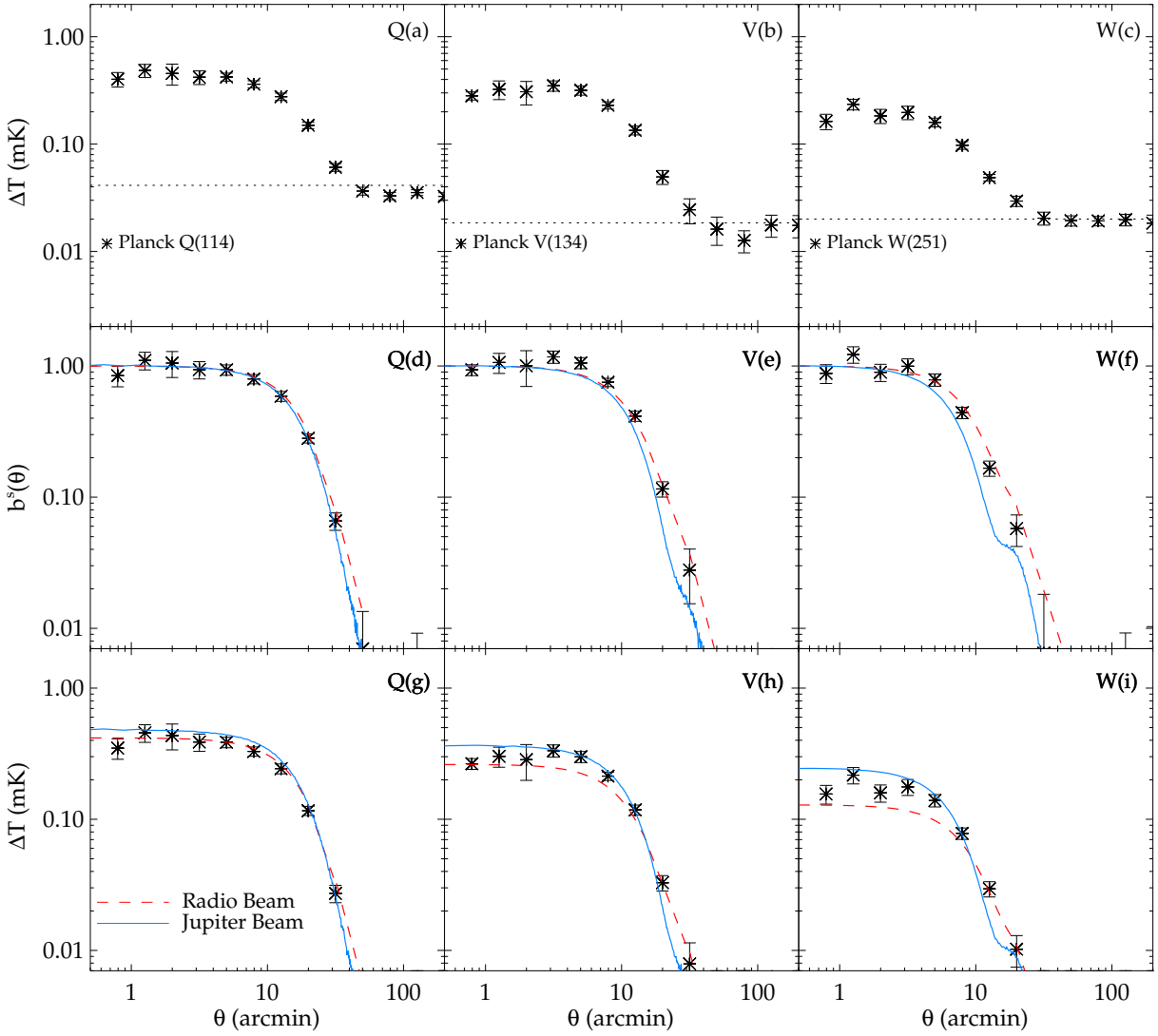

Figure 3. (a),(b),(c): The raw stacked *WMAP7* [Q,V,W] temperature profiles for the *Planck* [100,70,44] GHz band sources with the global mean temperature of the map plotted as the dashed line. (d),(e),(f): The photometrically subtracted, stacked and re-normalised *WMAP7* [Q,V,W] $b^s(\theta)$ profiles for the *Planck* [100,70,44] GHz band sources. Also shown are the $b^s(\theta)$ for the Jupiter beam (blue, solid) and the radio source fit (red, dashed) of Sawangwit & Shanks (2010a). (g),(h),(i): The photometrically subtracted stacked *WMAP7* [Q,V,W] $\Delta T(\theta)$ profiles for the *Planck* sources, now absolutely normalised via the *Planck* flux. Also shown are the $\Delta T(\theta)$ for the Jupiter beam (blue, solid) and the radio source fit (red, dashed) of Sawangwit & Shanks (2010a).

result further by using the CMB-free *WMAP* catalogue of Gold et al. (2011).

In the 'CMB-free' method, *WMAP* sources are selected using the Q,V, W bands simultaneously to form an internal linear combination map (ILC) with weights chosen to cancel out the CMB anisotropy signal. Again any Eddington bias due to CMB fluctuations should be reduced in the case of this new point source catalogue. We therefore repeated our stacking analysis with the 417 QVW sources from the Gold et al. 2011 *WMAP7* catalogue (see Fig. 5). Overall we again see wider-than-expected profiles, broadly consistent with the results in Figs. 3, 4 and the previous *WMAP5* results in Fig. 2 of Sawangwit & Shanks (2010a).

6.3 NVSS radio sources

Point source catalogues made at significantly lower frequencies than the *WMAP* bands are also unlikely to be affected by Eddington bias, if identification is done independently of the *WMAP7* point source catalogue. For example, point sources selected at 1.4 GHz will have Rayleigh-Jeans temperature $\approx 4500\times$ higher than a source with similar flux density selected at W-band (≈ 94 GHz), i.e. $T_{\rm RJ} \propto \Omega_{\rm beam}^{-1}\nu^{-2}$, whereas the rms Rayleigh-Jeans temperature due to the CMB fluctuations stays roughly the same between the two frequency bands, (Bennett et al. 2003). Therefore, we now stack *WMAP7* temperature data centred around the positions of the 1156 $S_{1.4} > 1$ Jy NVSS point sources. Fig. 6 shows the resulting Q1, V1 and W1 profiles. We see that

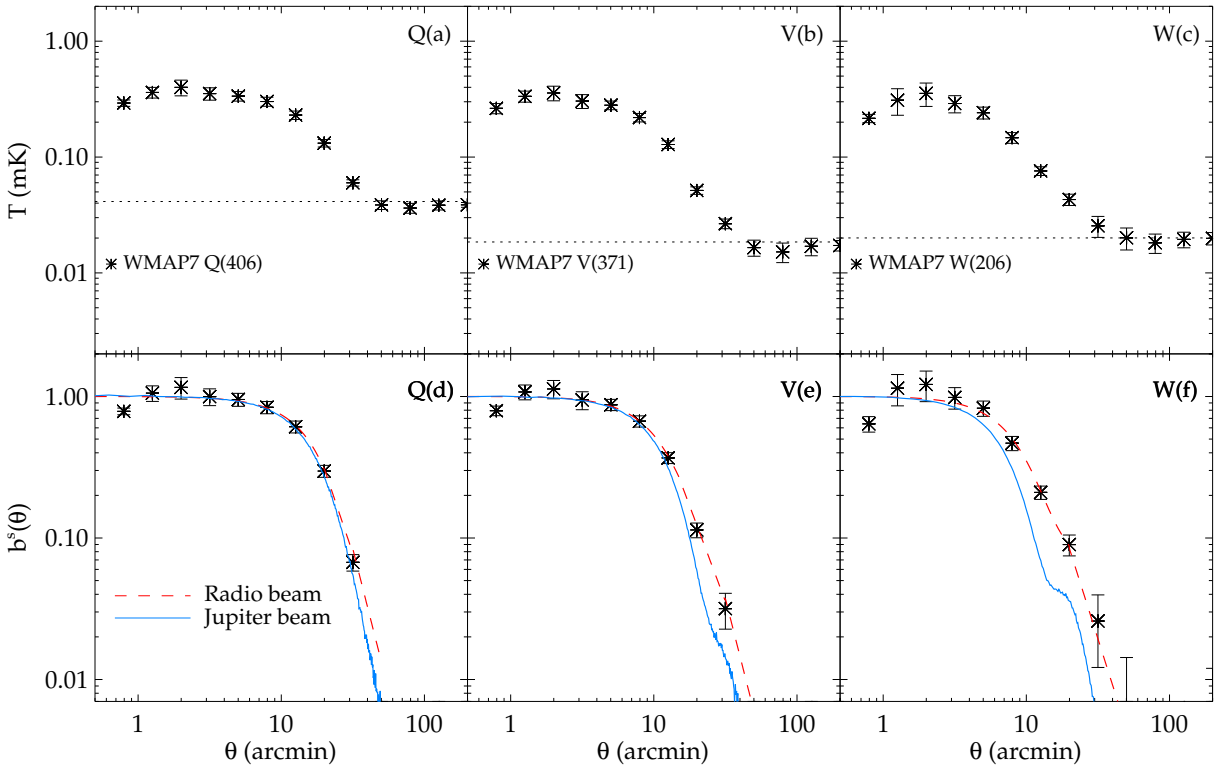

Figure 4. (a),(b),(c): The raw stacked *WMAP7* [Q,V,W] temperature profiles for the *WMAP7* sources of Gold et al. (2011) with the global mean temperature of the map plotted as the dashed line. (d),(e),(f): The photometrically subtracted, stacked and re-normalised *WMAP7* [Q,V,W] $b^s(\theta)$ profiles for the *WMAP7* sources of Gold et al. (2011). Also shown are the $b^s(\theta)$ for the Jupiter beam (blue, solid) and the radio source fit (red, dashed) of Sawangwit & Shanks (2010a).

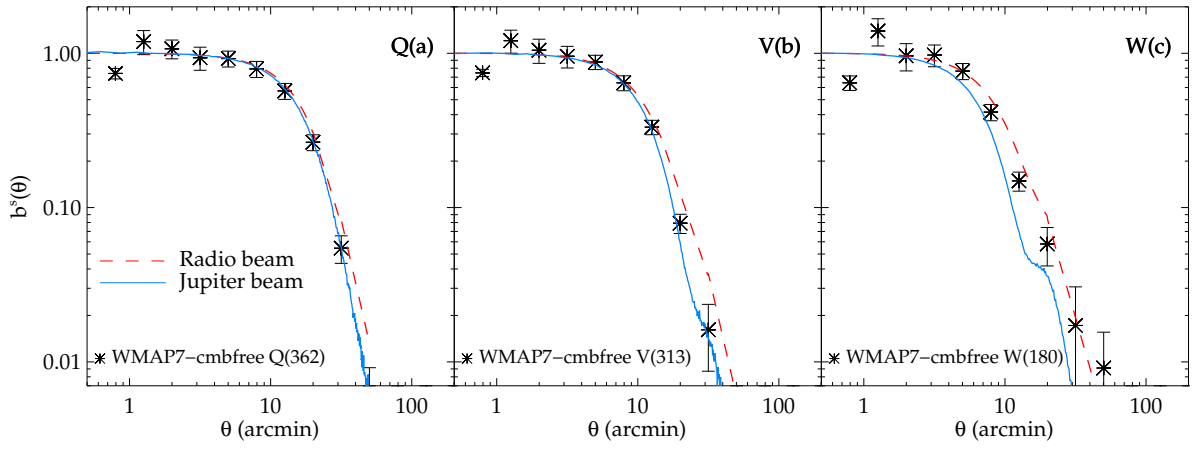

Figure 5. (a),(b),(c): The photometrically subtracted, stacked and re-normalised *WMAP7* [Q,V,W] $b^s(\theta)$ profiles for the CMB-free *WMAP* catalogues of Gold et al. (2011). Also shown are the $b^s(\theta)$ for the Jupiter beam (blue, solid) and the radio source fit (red, dashed) of Sawangwit & Shanks (2010a).

they are consistent with those measured using *WMAP5* total/bright sources in Fig. 2 of Sawangwit & Shanks (2010a). However, the profiles do not appear as wide as the *WMAP5* faintest subsample given that the average flux of the NVSS sample at *WMAP* bands is $\approx 3\times$ lower.

Many of the NVSS sources are resolved into multiple components (Blake & Wall 2002). However, this is unlikely to cause the widening of the beam beyond $\theta \gtrsim 6'$. Here, as a precautionary measure, we shall test the beam profile measured using the NVSS by excluding any source that

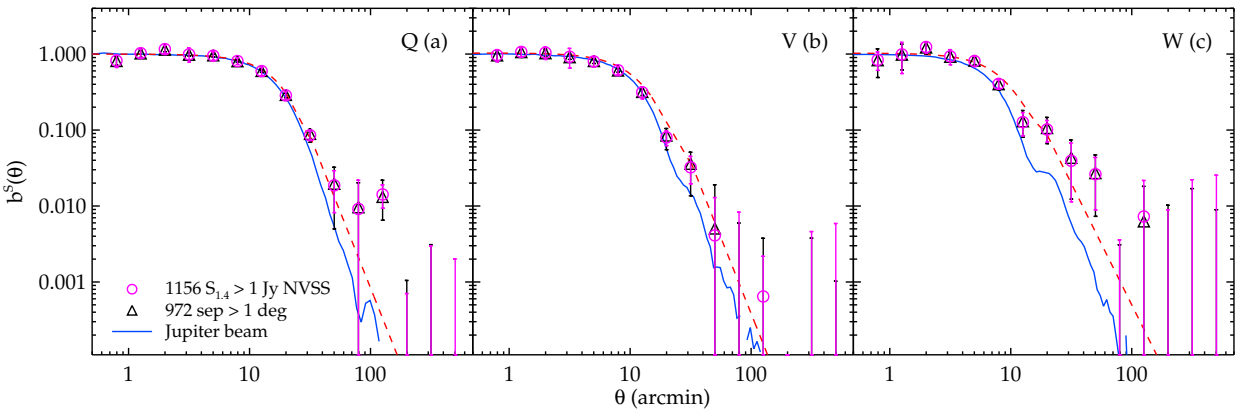

Figure 6. (a),(b),(c):The photometrically subtracted stacked WMAP7 [Q,V,W] $b^s(\theta)$ profiles for NVSS sources. Also shown are the $b^s(\theta)$ for the Jupiter beam (blue, solid) and the radio source fit (red, dashed) of Sawangwit & Shanks (2010a).

has neighbouring source(s) within 1°. This extra condition reduces the number of $S_{1.4} > 1.0$ Jy sources outside the *WMAP7* 'point source catalogue' mask to 972. The resulting beam profiles are also shown in the Fig. 6. We see that the beam profiles are in good agreement with the previous results.

7 RELATING *WMAP* FLUX NON-LINEARITY AND RADIO SOURCE PROFILES

Our first attempts to explain the wider than expected radio source profiles focused on the possibility that there was a timing offset between the *WMAP* antenna pointing and temperature data, as proposed by Liu & Li (2011). As well as causing effects at large scale due to a wrongly subtracted dipole, this scan pattern offset would cause a wider beam profile (see Moss, Scott, & Sigurdson 2011). However, Sawangwit et al (in prep) finds that while such an effect could help match the radio sources at $10'$ scales, it could not explain their profile at $30'$ unless the offset was significantly greater than 25.6ms in W band (≈ half a pixel) which may be unreasonable (Sawangwit et al in prep). Although this suggests that such an offset did not occur at the map-making stage, there is still the possibility that it could have occured at the calibration stage (Liu & Li 2011; Roukema 2010).

We now look instead for an explanation for the radio source beam profiles based on the non-linear *WMAP* radio-source fluxes and the wide beam profiles. We therefore take the power-law fits to the relations in Figs. 1 (a),(b,(c) and apply them to the symmetrised Jupiter beam $b^S(\theta)$ profiles which we assume is the true optical profile of the *WMAP* beam. The rationale for doing this is explained in Appendix B, where we assume that it is due to a non-linearity in the detector gain, $\widetilde{g} = k(\Delta T)^{-\alpha}$. So, taking the W band as an example, we applied the transformation $\widetilde{b}^S(\theta) = b^S_{Jupiter}(\theta)^{(1-\alpha)} = b^S_{Jupiter}(\theta)^{0.7}$, based on Fig. 1(a), to the W beam profile as measured from Jupiter to form the effective beam profile, $\widetilde{b}^S(\theta)$, for the W band.

The W band result is shown in Fig. 7 where it is compared to the error weighted mean of the empirical *WMAP*, NVSS and *Planck* profiles previously discussed. We see that the non-linear Jupiter beam appears to explain the radio source profiles very well over the full range of angles. This suggests there may be a direct connection between the flux non-linearity seen in Figs. 1 (a),(b),(c) and the wide radio source beam profiles. We also note that this 'non-linear beam' may even be starting to approach the so-called 'diy' beam reverse engineered to fit a particular cosmological model with a first acoustic peak at $l = 330$ (Sawangwit & Shanks 2010b).

Taking the *WMAP* estimate of the Jupiter beam as being accurate when at ≈ 1200Jy, which is significantly brighter than even the brightest ≈ 10Jy radio source we have used, is clearly an issue for the approach we have taken. Nevertheless, it is striking how well the average radio source profiles are reproduced when this assumption is made.

8 SZ RESULTS

8.1 *WMAP-Planck* SZ comparison

We next compare the stacked *WMAP7* temperature profiles for 159 clusters listed in the *Planck* ESZ catalogue. We are using the 'photometric' approach to background subtraction, with an annulus from $60' - 120'$ being used in W (and scaled according to beamwidth in Q and V). The self-similar models supplied by *Planck* as fits to the *Planck* data have been convolved with the *WMAP7* Jupiter beam in the first instance. We see in Fig. 8 that these models are poor fits to the *WMAP* data. In [W,V,Q] they lie a factor of ≈ [2.2, 2.4, 2.8] below the models at ≈ $10'$, with the discrepancy getting worse as we move to the lowest frequency Q and V bands. We also show similarly convolved isothermal models with parameters as listed in Section 3. Although the self-similar fits are lower than these at $60'$ scales and thus less discrepant with the *WMAP* data (Komatsu et al. 2011), the discrepancy of both the isothermal and self-similar models with the *WMAP* data remain poor at smaller scales. Of course, the main model here for inter-comparing *WMAP* and *Planck* is the self-similar model because that is the model fitted by the *Planck* team to their data.

We first tried to explain the SZ discrepancy via the

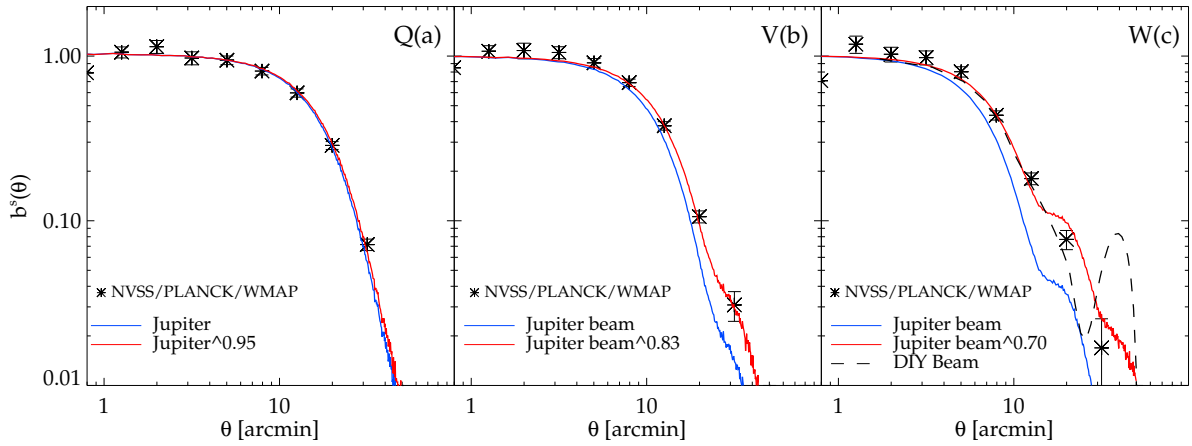

Figure 7. The weighted mean of the stacked radio source beams in the Q, V and W bands from *WMAP*, NVSS and *Planck* catalogues compared to the Jupiter beam (blue), and the 'non-linear Jupiter beam' (red) produced from applying the non-linear *WMAP-Planck* flux relation in Fig. 1(a) to the Jupiter beam. Also shown is the 'DIY' beam of Sawangwit & Shanks (2010b) reverse engineered from the raw *WMAP* C_l and the low H_0, $\Omega_{baryon} = 1$ model of Shanks (1985).

beam. In Figs. 8 we show the *Planck* self-similar models convolved with the power-law beams from Sawangwit & Shanks (2010a). We find that in the case of the W band where the radio source profiles are most different from the Jupiter beam, there is some improvement in the agreement with the *WMAP* data. But even here the deficit is reduced only by ≈ 20% in the centre. Indeed, at larger scales, the wider beams slightly worsen the agreement with *WMAP*. In the Q and V bands where the radio source profiles are closer to the Jupiter beam, the wider beams give virtually no improvement in the agreement with the *WMAP* data.

It is also the case that if we apply the non-linear flux-flux relation to the SZ profiles as we previously did to the radio profiles, we again see only a limited improvement in the agreement with the data. Again the *WMAP* SZ discrepancy is largest in Q where the radio source flux-flux non-linearity is smallest, arguing that a different explanation must apply to the *WMAP* SZ results.

8.2 Coma

We have also looked at the *Planck* model fits for the Coma cluster and compared them to *WMAP* (see Fig. 9). Part of the motivation here is that any beam problem may be expected to show up less for a nearby and therefore very extended ($\theta_{5R500} \approx 200'$) cluster like Coma, than in the case of more distant clusters. But here we see that the *Planck* model fit for Coma is now substantially *overestimated* by the *WMAP* data. This again argues that the explanation for the *Planck*-*WMAP* SZ discrepancy lies away from the beam profile.

Previously Lieu, Mittaz, & Zhang (2006) and Bielby & Shanks (2007) used an isothermal model to fit the Coma cluster. They used parameters estimated from the X-ray observations of Coma and found that the *WMAP* data could be fitted with these parameters. We show that this is still the case for the *WMAP7* data. The reason for the discrepancy with the self-similar fits to the *Planck* data is unknown. Komatsu et al. (2011) has discussed whether Coma may sit on a large downwards CMB fluctuation but clearly this cannot explain the *WMAP-Planck* discrepancy.

8.3 Explanations for the *WMAP-Planck* SZ discrepancies

First, we discuss whether the *WMAP* SZ discrepancy may instead be caused by degeneracies in the self similar model fits derived from the ESZ. One issue is that these fits are parameterised by the integrated quantity, $Y(5R_{500})$, yet the *WMAP* discrepancy is most significant at $\theta < 10'$ where the small solid angle reduces its contribution to $Y(5R_{500})$. However, the *Planck* fit is made by scaling the self-similar profile via an empirically measured central Compton parameter, y_0 (Melin, Bartlett, & Delabrouille 2006; Melin et al. 2011). Therefore y_0 is directly observed by *Planck*, suggesting that the small angle discrepancy may not be explained by an ambiguity in the ESZ SZ template.

Bielby & Shanks previously discussed the possibility that contamination of SZ clusters by radio sources could have reduced the *WMAP* SZ signal. Because *Planck* only use $\geqslant$ 100 GHz frequencies to identify SZ clusters, it could still be possible that the much smaller *WMAP* decrements seen at lower frequencies, particularly at Q(41 GHz), could be explained by radio source contamination only seen in the *WMAP* bands. However, the arguments against contamination previously applied by Bielby & Shanks to the W band almost equally apply to the V and Q bands; the contaminating sources found in low frequency (eg 30GHz) surveys by authors such as Coble et al. (2007) seem to have too low fluxes to explain the *WMAP* SZ discrepancy. In addition, when we exclude ≈ 10 ESZ clusters that have a contaminating 44, 70 or 100 GHz source within 1 degree, this was found to make little difference to our stacked SZ results in any of the *WMAP* bands.

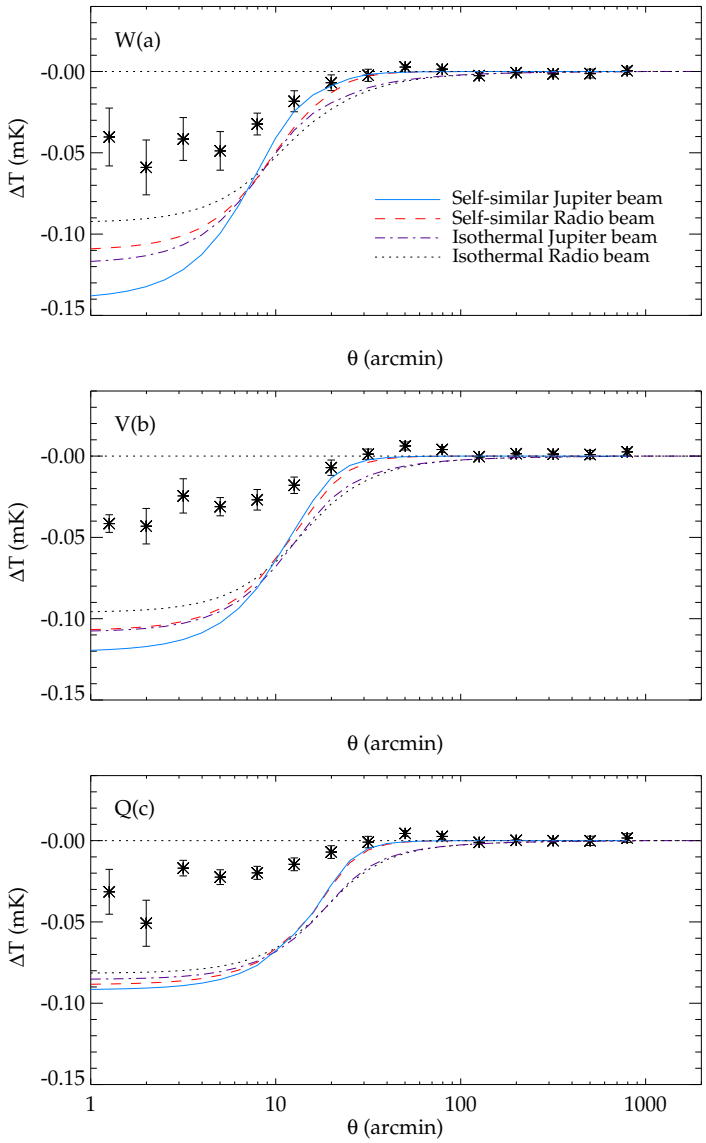

Figure 8. (a),(b),(c): The stacked SZ decrements of the *Planck* sources for the [W,V,Q] bands with the self-similar and isothermal β models convolved with a *WMAP* Jupiter beam and a beam fitted to the radio source profiles by Sawangwit & Shanks (2010a). The stacked *WMAP* SZ decrements are always significantly weaker than any of these *Planck*-based models.

We note that Bielby & Shanks (2007) already found a similar *WMAP* discrepancy with the SZ results of Bonamente et al. (2006) whose results are now weighted heavily to small scales because of the high resolution of these interferometric observations. We have checked a stack of 12 *Planck* SZ clusters that also belong to the Bonamente et al catalogue and find good agreement in their SZ decrements. These results argue that the *WMAP* SZ discrepancy at $\theta < 10'$ is replicated in comparisons with other experiments covering a wide range of scales, motivating us to look for an explanation in a systematic *WMAP* instrumentation error.

The large discrepancy seen at Q strongly argues that any systematics may be unrelated to the non-linear fluxes and wider beams measured for the radio sources. Since any optical beam profile effect must apply to both positive and negative ΔT equally, a more likely instrumental explanation could centre on different *WMAP* non-linearities at positive and negative ΔT (see Section 9).

9 DISCUSSION

The main criticism that was made of the previous results of Sawangwit & Shanks (2010a) was that the wide *WMAP* radio source profiles may be caused by Eddington bias

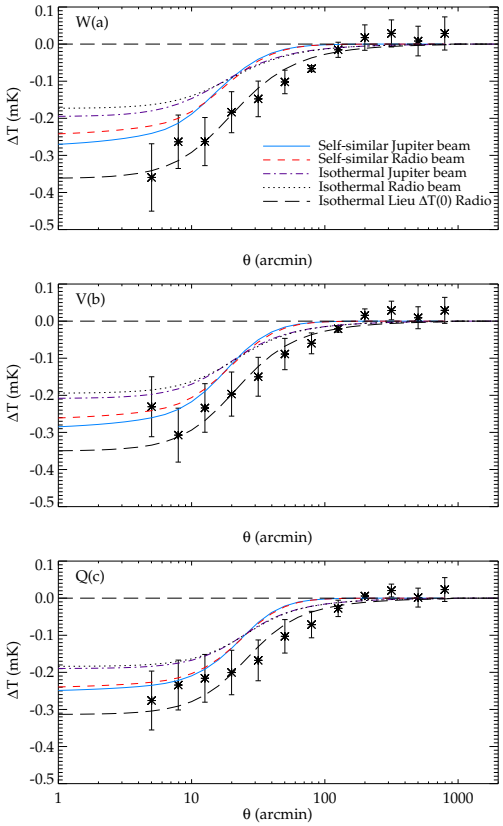

Figure 9. (a),(b),(c): The Coma SZ decrements for the [W,V,Q] bands with the self-similar and isothermal β models convolved with a *WMAP* Jupiter beam and a beam fitted to the radio source profiles by Sawangwit & Shanks (2010a). The error within each annulus for this individual cluster is simply the standard deviation of all clusters and is therefore only indicative. The observed *WMAP* decrements are now stronger than the *Planck* models and we also show an isothermal model based on the X-ray parameters used by Lieu, Mittaz, & Zhang (2006); Bielby & Shanks (2007), convolved with the radio profile beam and which fits the *WMAP* data well.

(Eddington 1913). Essentially, low S/N sources detected in *WMAP* data itself may be contaminated by upwards CMB fluctuations and not balanced by downwards fluctuations. This could explain the wider than expected profiles, particularly at faint fluxes.

There may be some evidence for Eddington bias in the faintest W band source sub-sample that was initially used by Sawangwit & Shanks (2010a), and for this reason the faintest sources were not used in their fits of the beam profile. Nevertheless, Eddington bias cannot affect sources detected at frequencies where CMB fluctuations are subdominant. We have found that NVSS selected sources at low frequency also show a wider beam at W. Also we note that the *Planck* sources show the wider beam independent of whether the CMBSUBTRACT flag applies. *WMAP* sources selected from a 'CMB-free' map also show the same wider than expected beam.

Furthermore, Sawangwit et al (in prep) ran Monte Carlo re-simulations of the source detection, producing artifical source catalogues extracted from simulated CMB maps. Here, after applying the same cross-correlation technique as for the data, the *WMAP* beam was recovered as input, again arguing that these sources are little affected by Eddington bias. These authors also argued that an offset in the *WMAP* scan pattern could contribute to widening the beam profile but only if the offsets were larger than previously dscussed by Liu & Li (2011) and then the fit at the largest, $30'$, scales could only be improved at the expense of the small-scale fit.

Importantly, the *Planck* data also confirms the non-linearity of *WMAP* fluxes, particularly in the W band. Decreasingly non-linear effects are also seen at Q and V. We have fitted this non-linearity and then applied the fit to the Jupiter beam profile. This procedure produced a surprisingly good fit to the radio-source profiles.

The interpretation of the comparison of *Planck*- *WMAP* SZ decrements is less clear. The possibility that this discrepancy is also due to a wider than expected *WMAP* beam profile is made less likely by the fact that the Q and V band discrepancies are at least as bad as at W, but the radio source profiles in these bands are much less discrepant than the profile at W. The *WMAP* SZ decrements are not only discrepant with the *Planck* decrements but also with the the OVRO SZ decrements of Bonamente et al. (2006). This suggests that the discrepancy may not be explained away by any degeneracies in the self-similar models that parameterise the *Planck* SZ results in the ESZ.

If the SZ discrepancy with *Planck* is real, then it is possible that there is a different gain dependence at negative ΔT than positive ΔT. The radio sources can only check the *WMAP* calibration at positive ΔT. Indeed, it is possible that the gain is linear although with a different gain constant given that dividing the *Planck* models by a factor of ≈ 2 appears to bring them into agreement with the *WMAP* SZ decrements.

It should be possible to test the calibration at both positive and negative ΔT by comparing the goodness of fit of a dipole model with a linear and non-linear gain with both the raw and calibrated counts and this work is in progress (Malik et al. in prep). A preference for a non-linear gain from the raw data would indicate non-linear detectors. Otherwise if the raw data showed a linear gain then it would suggest that any non-linearity had arisen during the combined calibration/map-making process.

We finally show in Fig. 10 the effect the 'non-linear beam', created via $\Delta\widetilde{T}(\theta) \propto \Delta T(\theta)^{0.7}$, (see Fig. 7c) has on the *WMAP* W1/W2 C_l. We assume here, for the moment, that this non-linear beam applies to both positive and negative ΔT. Then debeaming the raw W1/W2 C_l from PolSpice (Szapudi, Prunet, & Colombi 2001) via equns (1,2) of Sawangwit & Shanks (2010a), we see not only that the debeamed power spectrum (blue line in Fig. 10) is significantly higher in amplitude, but that the first peak has moved from $l = 220$ to $l = 275$ compared to the model debeamed using the Jupiter beam (cyan line). This is a similar effect as was reverse engineered by Sawangwit & Shanks (2010b) to fit the low H_0, $\Omega_b = 1$ cosmological model of Shanks (1985) where the peak occurs at $l = 330$. Here the black line represents the model and the red line the C_l resulting from debeaming with the 'diy' beam of Fig. 7. The fact that the *WMAP* C_l debeamed with the 'non-linear' Jupiter beam has

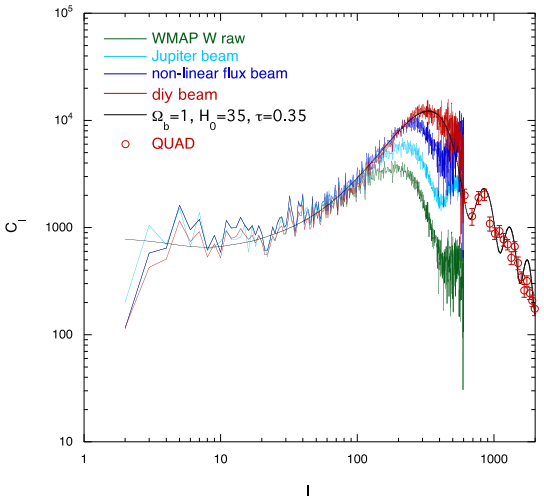

Figure 10. The *WMAP* W1/W2 raw C_l is shown as the green line. The usual C_l result from debeaming with the Jupiter beam is shown as the cyan line. The result produced by debeaming with the 'non-linear Jupiter beam' from Fig. 7 is shown as the blue line. The low H_0, $\Omega_{baryon} = 1$ model of Shanks (1985) is shown as the black line, together with the C_l reverse engineered from this model via the 'diy' beam, also from Fig. 7 (Sawangwit & Shanks 2010b) (red line). Also shown are the $l \gtrsim 600$ results from the QUAD experiment (Brown et al. 2009).

a first peak now approaching the position of this very simple model emphasises the importance of de-beaming to the cosmological interpretation of the *WMAP* power spectrum.

10 CONCLUSIONS

We have investigated the beam profile of *WMAP* by comparing beam profiles from radio sources with the Jupiter beam profile. We have compared sources from *Planck*, NVSS and *WMAP* CMB-free catalogues. We find that in all cases the radio sources show wider profiles than the Jupiter beam with little indication of Eddington bias or dependence on the method of normalisation. We have also found non-linearity in *WMAP* fluxes compared to *Planck* and ground-based fluxes. Moreover, we have now related the flux non-linearity to a gain non-linearity that can also explain the wide *WMAP* beam, particularly at W.

We have also compared stacked *WMAP* SZ decrements with those measured by *Planck* and by ground-based observations. Again, we find discrepancies with *WMAP* showing much lower decrements than observed in the *Planck* or in the ground-based data. The discrepancy is as large at Q as it is at W, arguing against an explanation involving the wide radio source profiles. We have suggested that there may be a different non-linear gain or at least a different linear gain that applies at negative ΔT.

We have shown that transforming the Jupiter beam using the non-linear radio source flux relation results in an significant change to the amplitude and position of even the first acoustic peak in the CMB power spectrum. At the least, a wider beam would imply a much larger uncertainty in the normalisation and hence the estimate of σ_8 from *WMAP*. Any uncertainty in the position of the first acoustic peak immediately translates into increased uncertainty in the CMB evidence for the CDM cosmological models. Clearly it is important to better understand the calibration and beam profile of *WMAP*, particularly in the W band which has the highest spatial resolution. Further tests using the dipole are currently being made on the raw and calibrated *WMAP* TOD to see if there is any suggestion that a non-linear gain solution may be preferred to a linear gain solution for the *WMAP* detectors (Malik et al. in prep).

ACKNOWLEDGMENTS

JRW acknowledges financial support from STFC. US acknowledges financial support from the Royal Thai Government. We acknowledge the use of data from NASA *WMAP* and ESA *Planck* collaborations.

REFERENCES

Arnaud M., Pratt G. W., Piffaretti R., Böhringer H., Croston J. H., Pointecouteau E., 2010, A&A, 517, A92
Bennett, C. L., et al. 2003, ApJS, 148, 97
Bennett C. L., et al., 2011, ApJS, 192, 17
Benson B. A., Church S. E., Ade P. A. R., Bock J. J., Ganga K. M., Henson C. N., Thompson K. L., 2004, ApJ, 617, 829
Bielby R. M., Shanks T., 2007, MNRAS, 382, 1196
Blake C., Wall J., 2002, MNRAS, 337, 993
Bonamente M., Joy M. K., LaRoque S. J., Carlstrom J. E., Reese E. D., Dawson K. S., 2006, ApJ, 647, 25
Brown M. L., et al., 2009, ApJ, 705, 978
Cavaliere A., Fusco-Femiano R., 1976, A&A, 49, 137
Chen X., Wright E. L., 2009, ApJ, 694, 222
Coble K., et al., 2007, AJ, 134, 897
Dawson K. S., Holzapfel W. L., Carlstrom J. E., Joy M., LaRoque S. J., 2006, ApJ, 647, 13
Diego J. M, Partridge B., 2009, arXiv, arXiv:0907.0233
Eddington A. S., 1913, MNRAS, 73, 359
Gold B., et al., 2011, ApJS, 192, 15
Gregory P. C., Scott W. K., Douglas K., Condon J. J., 1996, ApJS, 103, 427
Griffith M. R., Wright A. E., 1993, AJ, 105, 1666
Hill R. S., et al., 2009, ApJS, 180, 246
Jarosik N., et al., 2003, ApJS, 145, 413
Jarosik N., et al., 2011, ApJS, 192, 14
Komatsu E., et al., 2011, ApJS, 192, 18
Lange A. E., et al., 2001, PhRvD, 63, 042001
Lieu R., Mittaz J. P. D., Zhang S.-N., 2006, ApJ, 648, 176
Liu H., Li T.-P., 2011, ApJ, 732, 125
Lueker M., et al., 2010, ApJ, 719, 1045
MacTavish C. J., et al., 2006, ApJ, 647, 799
Malik, Sawangwit U., Shanks T. & Whitbourn, J., 2011, In preparation
Melin J.-B., Bartlett J. G., Delabrouille J., Arnaud M., Piffaretti R., Pratt G. W., 2011, A&A, 525, A139
Melin J.-B., Bartlett J. G., Delabrouille J., 2006, A&A, 459, 341
Miller A. D., 2002, grg..conf, 241
Moss A., Scott D., Sigurdson K., 2011, JCAP, 1, 1
Mroczkowski T., et al., 2009, ApJ, 694, 1034

Myers A. D., Shanks T., Outram P. J., Frith W. J., Wolfendale A. W., 2004, MNRAS, 347, L67
Nagai D., Vikhlinin A., Kravtsov A. V., 2007, ApJ, 655, 98
Page L., et al., 2003, ApJS, 148, 39
Page L., et al., 2003, ApJ, 585, 566
Piffaretti R., Jetzer P., Kaastra J. S., Tamura T., 2005, A&A, 433, 101
Planck Collaboration, et al., 2011, arXiv, arXiv:1101.2024
Planck Collaboration, et al., 2011, arXiv, arXiv:1101.2043
Planck Collaboration et al. 2011, ESA
Pratt G. W., Böhringer H., Croston J. H., Arnaud M., Borgani S., Finoguenov A., Temple R. F., 2007, A&A, 461, 71
Refregier A., Spergel D. N., Herbig T., 2000, ApJ, 531, 31
Roukema B. F., 2010, arXiv, arXiv:1007.5307
Sawangwit U., Shanks T., 2010a, MNRAS, 407, L16
Sawangwit U., Shanks T., 2010b, In '45th Rencontres de Moriond: Cosmology 2010', Eds Auge, E., Dumarchez, J. & Tran Thanh Van, J., pp. 53-57, GIOI: Vietnam, (arXiv:1006.1270).
Sawangwit U., et al, 2011, In preparation.
Shanks T., 1985, Vistas in Astr., 28, 595
Shaw L. D., Nagai D., Bhattacharya S., Lau E. T., 2010, ApJ, 725, 1452
Szapudi I., Prunet S., Colombi S., 2001, ApJ, 561, L11
Veneziani M., et al., 2009, ApJ, 702, L61
Wright E. L., et al., 2009, ApJS, 180, 283

APPENDIX A: SZ SELF SIMILAR MODEL

In the self-similar SZ model as employed in the *Planck* ESZ, the fundamental parameters of a cluster are P_{500}, M_{500} and R_{500}. Using the terminology of Arnaud et al. (2010),

$$M_{500} = \frac{4\pi}{3} R_{500}^3 500 \rho_{crit} \tag{A1}$$

$$R_{500} = D_a(z) \frac{\theta_{5R_{500}}}{5} \tag{A2}$$

A Y_{500} parameter corresponding to these is also defined,

$$Y_{500} = \frac{\sigma_t}{m_e c^2} \frac{4\pi R_{500}^3}{3} P_{500} \tag{A3}$$

which can be used as a characteristic SZ parameter instead of P_{500}. In equn. (A3) the units of Y_{500} are Mpc^2, but are easily convertible to the arcmin^2 units used in ESZ and throughout this paper[4]. This Y_{500} is a distinct quantity from $Y(R_{500})$ as found by evaluating equn. (9), In fact both P_{500} and Y_{500} ultimately cancel out of our calculation of the integral $Y_{cyl}(< R)$, from the *Planck* provided parameters, the fully integrated Y_{5R500} and $\theta_{5R_{500}}$.

However, the introduction of Y_{500} is well motivated because, as shown by Arnaud et al. (2010), it allows a scale-free description of Y_{sph} and Y_{cyl} in terms of $x = R/R_{500}$ as follows,

$$Y_{sph}(x) = Y_{500} I(x), \tag{A4}$$

$$Y_{cyl}(x) = Y_{sph}(5R_{500}) - Y_{500} J(x) \tag{A5}$$

where $I(x)$ and $J(x)$ are the spherical and cylindrical scaling functions,

$$I(x) = \int_0^x 3\mathcal{P}(u) u^2 du, \tag{A6}$$

$$J(x) = \int_x^5 3\mathcal{P}(u)(u^2 - x^2)^{1/2} u du. \tag{A7}$$

We therefore find that

$$Y_{cyl}(x) = Y_{500}(I(5) - J(x)), \tag{A8}$$

and since $Y_{cyl}(5) = Y_{sph}(5) = I(5) Y_{500}$ we finally obtain

$$Y_{cyl}(R) = Y_{cyl}(5R_{500}) \left(1 - \frac{J(x)}{I(5)}\right) \tag{A9}$$

APPENDIX B: FLUX NON-LINEARITY

The *WMAP* team assumption is that the detector gain, g, is independent of temperature and then that $c_{raw} = g \times \Delta T + b$ where c_{raw} is the raw differential count and b is the baseline. We now assume a non-linear gain $\widetilde{g} = k\Delta T^{-\alpha}$. Then if the raw detector counts, $\widetilde{c}_{raw}$, are $\widetilde{c}_{raw} = \widetilde{g}\Delta T$, (subsuming the baseline, b, into c_{raw}) then the recovered ΔT assuming a linear gain is

$$\Delta\widetilde{T} = \widetilde{c}_{raw}/g = \widetilde{g}\Delta T/g \Rightarrow \Delta\widetilde{T} = k\Delta T^{1-\alpha}/g$$

[4] $Y[Mpc^2] = \frac{1}{60^2}(\frac{\pi}{180})^2 (D_a[Mpc])^2 Y[arcmin^2]$

If $\Delta T_a(\theta) = \Delta T_a^0 b^S(\theta)$ where $\Delta T_a^0(\theta)$ is the central antenna temperature and $b^S(\theta)$ is the true beam profile normalised to unity at the centre, then

$$\Delta\widetilde{T}_a(\theta) \propto \Delta T_a(\theta)^{(1-\alpha)} = {\Delta T_a^0}^{(1-\alpha)} b^S(\theta)^{(1-\alpha)} = \Delta\widetilde{T}_a^0 \widetilde{b}^S(\theta)$$

Since $b^S(0) = 1$, $\Delta\widetilde{T}_a^0 = {\Delta T_a^0}^{(1-\alpha)}$, so $\widetilde{b}^S(\theta) = b^S(\theta)^{(1-\alpha)}$ i.e. if the gain is non-linear to the power, $-\alpha$, then a point source profile will be non-linear to the power, $(1-\alpha)$.

Next we look at what the above non-linear gain relation means for fluxes. The relation between central antenna temperature and flux, S_ν, is

$$\Delta T_a^0 = \frac{S_\nu}{\Omega_B}\frac{\partial B_\nu}{\partial T} \times \frac{1}{g(\nu)} = S_\nu \Gamma_\nu$$

Therefore $S_\nu = \Delta T_a^0/\Gamma_\nu$ and $\widetilde{S}_\nu = \Delta\widetilde{T}_a^0/\widetilde{\Gamma}_\nu$ where $1/\widetilde{\Gamma}_\nu = \widetilde{\Omega}_B \frac{\partial B_\nu}{\partial T} g(\nu)$. By using the Jupiter beam to convert peak temperature to a flux S_ν, *WMAP* have effectively assumed $\widetilde{\Omega}_B = \Omega_B$ and therefore $\widetilde{\Gamma} = \Gamma$ and so,

$$S_\nu/\widetilde{S}_\nu = \Delta T_a^0/\Delta\widetilde{T}_a^0 = {\Delta T_a^0}^\alpha = S_\nu^\alpha \Gamma_\nu^\alpha$$

Hence $\widetilde{S}_\nu = S_\nu^{(1-\alpha)}\Gamma_\nu^{-\alpha}$. So a non-linear gain with a $\Delta T^{-\alpha}$ temperature dependence produces non-linearity in both the radio profiles and the flux scale to the $(1-\alpha)$ power.

This paper has been typeset from a TEX/ LATEX file prepared by the author.